Structural Analysis of Alzheimer's β(1–40) Amyloid: Protofilament Assembly of Tubular Fibrils

Sergey B. Malinchik, Hideyo Inouye, Karen E. Szumowski, and Daniel A. Kirschner
Department of Biology, Boston College, Chestnut Hill, Massachusetts 02167-3811 USA

ABSTRACT Detailed structural studies of amyloid fibrils can elucidate the way in which their constituent polypeptides are folded and self-assemble, and exert their neurotoxic effects in Alzheimer's disease (AD). We have previously reported that when aqueous solutions of the N-terminal hydrophilic peptides of AD β-amyloid (Aβ) are gradually dried in a 2-Tesla magnetic field, they form highly oriented fibrils that are well suited to x-ray fiber diffraction. The longer, more physiologically relevant sequences such as Aβ(1–40) have not been amenable to such analysis, owing to their strong propensity to polymerize and aggregate before orientation is achieved. In seeking an efficient and inexpensive method for rapid screening of conditions that could lead to improved orientation of fibrils assembled from the longer peptides, we report here that the birefringence of a small drop of peptide solution can supply information related to the cooperative packing of amyloid fibers and their capacity for magnetic orientation. The samples were examined by electron microscopy (negative and positive staining) and x-ray diffraction. Negative staining showed a mixture of straight and twisted fibers. The average width of both types was ~70 Å, and the helical pitch of the latter was ~460 Å. Cross sections of plastic-embedded samples showed a ~60-Å-wide tubular structure. X-ray diffraction from these samples indicated a cross-β fiber pattern, characterized by a strong meridional reflection at 4.74 Å and a broad equatorial reflection at 8.9 Å. Modeling studies suggested that tilted arrays of β-strands constitute tubular, 30-Å-diameter protofilaments, and that three to five of these protofilaments constitute the Aβ fiber. This type of structure—a multimeric array of protofilaments organized as a tubular fibril—resembles that formed by the shorter Aβ fragments (e.g., Aβ(6–25), Aβ(11–25), Aβ(1–28)), suggesting a common structural motif in AD amyloid fibril organization.

INTRODUCTION

One of the fundamental problems in Alzheimer's disease (AD) research is to determine what drives the formation of amyloid fibrils from specific polypeptide fragments of the Aβ precursor protein. Amyloid fibrils and their accumulation as deposits in the neuropil can profoundly affect the functioning of the central nervous system, perhaps by neurotoxic mechanisms (Mattson and Rydel, 1996). To characterize the way in which the peptides assemble and exert their effects, we have been studying in vitro fibrilogenesis by using x-ray fiber diffraction and electron microscopy. We found that highly oriented fibrils for x-ray diffraction could be attained by gradually drying the peptide solution in a 2-Tesla magnetic field (Inouye et al., 1993, and references cited therein). Our previous experiments mainly utilized peptide fragments corresponding to the putative extracellular domain of Aβ, although some 40-mers were also studied, including primate, rodent, and Dutch-hemorrhagic analogs (Fraser et al., 1992). The difficulty in undertaking fiber diffraction from the longer, more physiologically relevant peptides is that, unlike most of the shorter peptides, the assembled fibers do not easily orient in a magnetic field. This results in more overlap among the x-ray reflections, making, in turn, the diffraction patterns considerably more difficult to interpret. However, because the 1–40 and 1–42 fragments are the major polypeptides found in amyloid deposits in AD, we have sought improved methods for producing from the full-length peptides oriented samples that are suitable for x-ray fiber diffraction.

The general poblem of preparing oriented fiber samples was recognized over 50 years ago in the pioneering work of Bernal and Fankuchen (1941) with tomato mosaic virus fibers. The significance of our current study arises not only because the highly ordered structure can be analyzed more easily by x-ray diffraction, but also the assembly process itself (from soluble peptide to insoluble fibers) may simulate a portion of the pathophysiological process leading to fibril formation in AD brains. Given that the fibrillar form as opposed to the soluble form may exert neurotoxicity, such as oxidant stress and activation of microglia (Mattson and Rydel, 1996), the molecular structural information of the fibrillar and soluble forms of the full sequence 1–40 may be fundamental to understanding neurodegeneration. One of the questions addressed here, therefore, pertains to that feature of the molecular organization of Aβ(1–40), which exerts the cytotoxic effects.

In the current study, a "drop test" using polarized light microscopy was newly developed to quickly test whether the peptides treated under different conditions can be oriented into well-aligned fibers. Birefringent samples were subsequently examined in the electron microscope and by x-ray diffraction. We demonstrate here that assemblies of Aβ(1–40) can become well oriented in a magnetic field after the bulk peptide solution is stored in the refrigerator for several months. Electron microscopy indicates that the

Received for publication 11 March 1997 and in final form 27 May 1997.
Address reprint requests to Dr. Daniel A. Kirschner, Department of Biology, Boston College, 140 Commonwealth Avenue, Chestnut Hill, MA 02167-3811. Tel.: 617-552-0211; Fax: 617-552-2011; E-mail: daniel.kirschner@bc.edu.

0006-3495/98/01/537/09 $2.00

peptides formed both twisted fibers of average diameter ~70 Å and pitch 460 Å, and straight fibers with the same diameter. Modeling the fibril structure from the x-ray diffraction data indicated that the fibril was tubular and was formed by a multimeric array of protofilaments.

MATERIALS AND METHODS

Aβ(1–40) peptide

We tested Aβ(1–40) peptides from three different sources: Bachem California (Torrance, CA; lot number ZM365; peptide purity >99% by HPLC); Dr. David B. Teplow (custom synthesized at Harvard Medical School; peptide purity is >99% by diphenyl reverse phase-HPLC, and ~92% by RP-HPLC) on a PLRP-5 column (Polymer Laboratories, Amherst, MA); and Quality Controlled Biochemicals (Hopkinton, MA; lot number 03013608; peptide purity >99% by HPLC; peptide provided by Dr. John E. Maggio).

Dry drop test by polarized light microscopy

Owing to the high cost of synthetic peptides and our need to survey a variety of conditions for peptide assembly and orientation, we sought to develop a method that utilizes microgram quantities of peptide for rapid screening. We found that examining the birefringence of a small drop of peptide solution could supply information related to the aggregation properties of β-amyloid fibers and their capacity for orientation in a magnetic field. Thus, 0.5-μl-aliquot drops of amyloid peptide solutions at concentrations of 5–10 mg/ml were allowed to dry on siliconized glass surfaces. The protein tends to concentrate along the circular border at the liquid-glass interface. Birefringence of the dried drop was checked by a polarizing microscope.

We tested a number of available short β-amyloid fragments and compared the results with their corresponding x-ray diffraction patterns (see Inouye et al., 1993). For all fragments tested, which included Aβ(11–28), Aβ(13–28), Aβ(11–25), Aβ(9–28), and Aβ(19–28), we found a clear correlation between the extent of birefringence in the dry drop and the quality of the peptide orientation in a magnetic field. The latter, which we term "crystallinity," was judged from the mosaic spread of the x-ray reflections and the presence of Bragg reflections on layer lines.

Electron microscopy

For thin sectioning, peptide samples were dissolved in water at 10 mg/ml and concentrated by evaporation to ~200 mg/ml. The resulting peptide gels were fixed by exposure to glutaraldehyde vapor and then to osmium tetroxide vapor. Subsequently, the gels were immersion-fixed in 2% glutaraldehyde (aq.) and 2% osmium tetroxide (aq.), stained en bloc with 4% uranyl acetate in 50% ethanol, dehydrated through a series of ethanols and propylene oxide, and embedded in Poly Bed 812. The sections were viewed in a JEOL 1200 EX electron microscope at 120 kV.

For negative staining, peptide solutions at concentrations of ~2 mg/ml were placed on carbon-coated, Formvar-covered copper grids, fixed with 0.5% glutaraldehyde and stained with 2% (wt/vol) uranyl acetate. Samples were observed in a JEOL 1200 EX electron microscope operated at 120 kV. Calibration of the micrographs was carried out with tropomyosin paracrystals (kindly provided by Dr. Carolyn Cohen, Brandeis University, Waltham, MA).

X-ray diffraction

Sample

Peptide solutions at ~5 mg/ml in distilled water were stored in the refrigerator for a few days to a few months. The samples for x-ray diffraction experiments were prepared as detailed previously (Inouye et al., 1993). Briefly, the peptide solutions were introduced into siliconized glass capillaries, which were then placed in 2-Tesla permanent magnets (Oldenbourg and Phillips, 1986) and allowed to dry under ambient temperature and humidity.

Data collection

X-ray patterns were collected using nickel-filtered and double-mirror-focused CuKα radiation from a GX-6 rotating-anode x-ray generator (Elliott-Marconi Avionics, Hertfordshire, England) with a 200-μm focal spot, and operated at 30 kV and 40 mA. A helium tunnel was placed in the x-ray path to reduce air scatter. Patterns were recorded on flat, direct-exposure x-ray film (Eastman Kodak) for 1–3 days. The specimen-to-film distance was 71.8 mm, as calibrated by the known spacings of NaCl (3.258 Å and 2.821 Å).

Densitometry and measurement of the intensity

Densitometry to quantitate the intensities was carried out as previously described (Nguyen et al., 1995). Briefly, diffraction patterns were digitized on a 100-μm raster using a VEXCEL scanner operated by the program VXSCAN. The two-dimensional intensities were displayed with SCOPE5 (Tibbitts and Caspar, 1993). The intensity curve was obtained after subtraction of the background, which was fit by polynomial or exponential equations. For precise measurement of the spacings of the reflections, the corresponding intensity peaks were fit by a Gaussian function with the program PeakFit (Jandel Scientific Software).

Model calculations

The equatorial diffraction patterns were calculated according to $I(R) = F^2(R)Z(R)/NR$. Here N is the number of subunits, $F(R) = 2\pi[r_1J_0(2\pi r_1R) + r_2J_0(2\pi r_2R)]$, where r_1 and r_2 are the outer and inner radii of a thin-walled cylinder, and $Z(R) = \Sigma_j\Sigma_k J_0(2\pi r_{jk}R)$, where $r_{jk} = |\mathbf{r}_j - \mathbf{r}_k|$ for the distance between the subunit vectors in cylindrical coordinates (Vainshtein, 1966). The denominator R corrects for the mosaic spread of the intensity, because the observed intensity was derived from a strip scan along the equator.

RESULTS

Conditions for sample preparation

The drop test for the Aβ(1–40) peptides was carried out systematically to seek promising conditions for fiber growth and orientation. As a positive control, we used peptide Aβ(11–25), which, when fibrillar, orients readily in a magnetic field and gives sharp x-ray diffraction (Inouye et al., 1993), and gives very strong birefringence in the drop test. When lyophilized peptides from the three different sources of Aβ(1–40) (see Materials and Methods) were dissolved in distilled water and incubated at 24°C for 3–5 days, all showed very poor birefringence in the drop test (Fig. 1, *a* and *b*), and the concentrated samples prepared from these peptide solutions did not show any response to a 2-T magnetic field, as judged by the lack of orientation of birefringent domains during the drying period. X-ray diffraction patterns from the partially dried pellets showed very poor orientation, with only weak reflections suggestive of a cross-β structure. Variations in the initial conditions—including peptide concentrations (from 0.1 to 10 mg/ml), pH (range, pH 5–9) (Fraser et al., 1991b), ionic strength, and

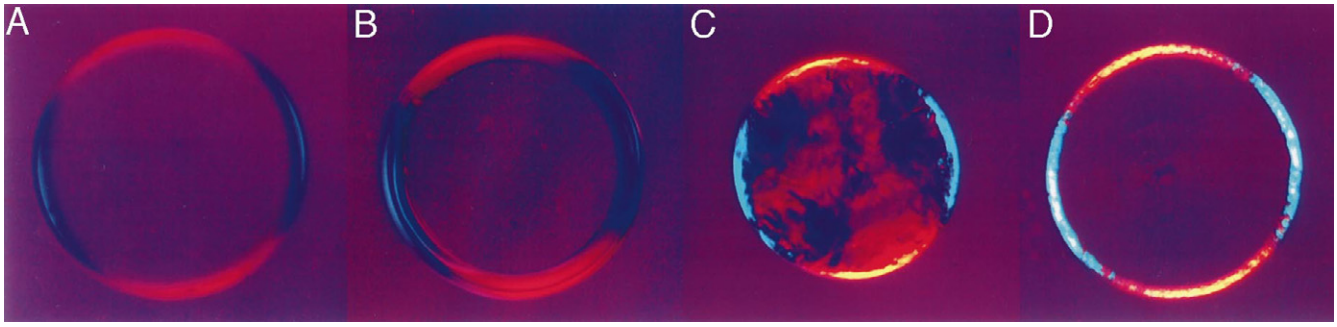

FIGURE 1 Results of the drop test. Images of dried drops of peptide solutions, viewed between crossed polarizers, suggest whether liquid crystalline domains have formed in the peptide solutions. (*A* and *B*) Aβ(1–40) peptide solutions (5 mg/ml) from different peptide sources (Bachem (*A*) and QCB (*B*)) up to 30 days after dissolving in distilled water. Birefringence is absent or very weak. (*C*) Aβ(1–40) peptide (QCB) after 3 months' storage in the cold shows strong birefringence. (*D*) Aβ(11–25) peptide a few hours after dissolving in water indicates strong birefringence. While drying under ambient conditions, the peptide solutions of *C* and *D* showed birefringent domains that could be oriented in a 2-T magnetic field.

presence of sulfate ions (Fraser et al., 1992)—did not improve the ability of the fibers to orient in the magnetic field. Indeed, electron microscopy invariably showed the formation of unbranched, typical-looking fibers with considerable variation in length.

The idea of exploring the time factor in fiber formation was based on the finding that aqueous solutions of peptide Aβ(1–40) synthesized by Quality Controlled Biochemicals (QCB, Hopkinton, MA) are higly monomeric and stable (Dr. John E. Maggio, personal communication). Because previous reports have shown that storage of Aβ peptides at low concentration leads gradually to changes in their secondary structure and aggregation properties (Barrow and Zagorski, 1991; Barrow et al., 1992; Pike et al., 1991a,b), we thought it worthwhile to monitor fiber formation and magnetic orientation in peptide preparations that were known to be relatively stable.

After the QCB peptide solution was kept at an initial concentration of 5 mg/ml in the refrigerator for three months, the drop test revealed a strong birefringence comparable to that shown for Aβ(11–25). Fig. 1, *b* and *c*, illustrates the drop tests for Aβ(1–40) at 10 days and at 3 months after lyophilized peptide is dissolved in water. Drop tests after 1 and 2 months did not show any difference from that at 10 days. By contrast, the drop test for Aβ(11–25) 1 h after the peptide was dissolved in water showed prominent birefringence (Fig. 1 *d*).

Samples used for electron microscopy and x-ray diffraction were preparations of Aβ(1–40) from QCB that had been stored for 3 months in the refrigerator. During drying in the capillary tube, the peptide solution showed birefringent domains that could be oriented in the 2-T magnetic field. The resulting thin pellet could be rotated to show uniform extinction when viewed face on, and was used for fiber diffraction (see Fig. 2).

Fiber structure of Aβ(1–40) observed by electron microscopy

Negative staining of QCB Aβ(1–40) samples showed long, unbranched fibers. There was considerable variation in the appearance of the fiber structure, even on the same grids. Generally, the fibrillar assemblies could be divided into two main populations: one consisting of narrow, straight fibers, and the other consisting of twisted, paired fibers (Fig. 3, *a*

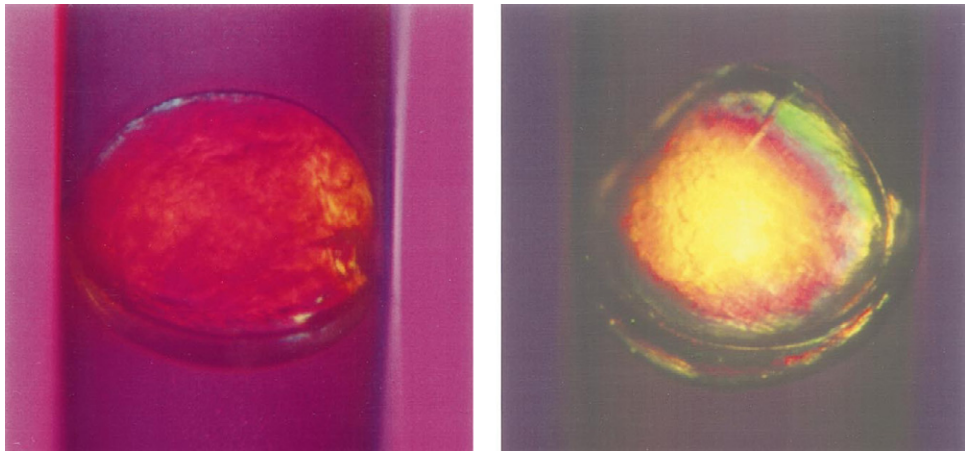

FIGURE 2 The final pellets formed by peptide solutions *C* and *D* of Fig. 1. (*left*) Aβ(1–40); (*right*) Aβ(11–25). Viewed through a polarizing microscope, the samples show uniform extinction.

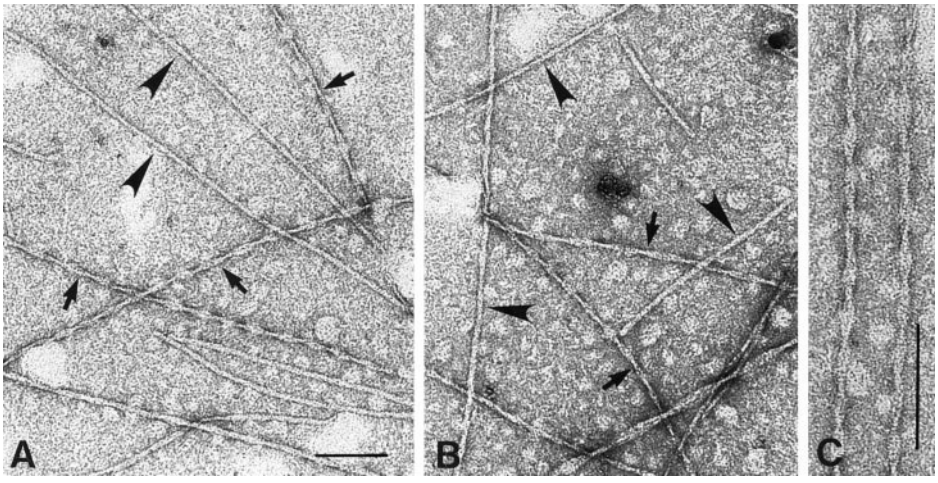

FIGURE 3 Electron micrographs of negative-stained preparations. (*A* and *B*) "Aged" Aβ(1–40) samples (QCB peptide) exhibited a multitude of long fibers, falling primarily into one of two types: regularly twisted fibers (*arrows*) and straight, relatively smooth fibers (*arrowheads*). Scale bar, 1000 Å. (*C*) Higher magnification of two twisted fibers from an "aged" sample of QCB Aβ(1–40). Scale bar, 1000 Å.

and *b*). The average fiber size for both types of structures was ~70 Å (range, 60–80 Å for smooth fibers and 50–90 Å for twisted fibers). The helical pitch of the twisted fibers was ~460 Å (range, 360–560 Å). Cross-sectioned samples of another sample (Aβ(1–40) sythesized in the laboratory of Dr. David Teplow (Harvard Medical School) (Fig. 4) showed a tubular structure, ~60 Å in diameter, with an electron-lucent center. Although there were discrete deposits of staining along the circular wall of the fiber, indicating possible subunit structures, the number of subunits constituting the tubular wall was not unambiguous from the electron micrographs.

X-ray results and interpretation

The highly birefringent Aβ(1–40) sample gave a cross-β diffraction pattern (Fig. 5) in which a sharp 4.7-Å reflection was on the meridian, and a broad 8.9-Å reflection was on the equator. In most cross-β patterns from β-amyloid analogs, an off-meridional 3.8-Å reflection is observed, but here the intensity maximum for this reflection was on the meridian. We also observed in the low-angle region a very strong and sharp equatorial reflection at 49.2 Å and two broad reflections at 19.0 Å and 13.7 Å.

Meridional diffraction

Different β-amyloid analogs appear to have in common an orthogonal unit cell with characteristic dimensions of $a \approx 9.4$ Å, $b \approx 6.6$ Å, and $c \approx 10$ Å (Inouye et al., 1993), where the *a* axis is parallel to the hydrogen bonding direction, *b* is along the chain direction, and *c* is along the intersheet direction. For the Aβ(1–40) considered here, the observed reflections on the meridian at 4.72 Å and 3.84 Å, and on the equator at 8.9 Å, were indexed as (200), (210), and (001) of the orthogonal unit cell, with $a = 9.44$ Å, $b = 6.60$ Å, and $c = 8.9$ Å.

When the fiber is aligned with the *a* axis parallel to the fiber direction, as in a classical cross-β pattern (Geddes et al., 1968), the (200) is strictly meridional, whereas the (210) is off-meridional, and the β-chains are perpendicular to the fiber axis. For the case of Aβ(1–40) previously described (Fraser et al., 1992), the (200) and the (210) were clearly off-meridional and on the meridian, respectively, indicating that the β-chains are tilted by 35.6° (*acos*(3.84/4.72)) from their perpendicular orientation. In the pattern for Aβ(1–40) described here, both the (200) and the (210) reflections appear to be on the meridian. This may be explained by rotation around the fiber axis (cylindrical averaging), which enhances the relative intensity of the meridional reflections relative to the off-meridional ones, and by translational and angular disorders within the fibers, which broaden the off-meridional reflections on the layer lines but not on the meridian and equator (Inouye, 1994).

Equatorial diffraction

The equatorial scattering and reflections arise from the axial projection of the electron density distribution. The primary peak at 49.2 Å was very sharp and strong, whereas the subsequent peaks at 19.0, 13.7 and 8.9 Å were weak and broad. The first peak can be regarded as arising from interference between objects arranged laterally on a short-range, two-dimensional lattice. If the 49.2 Å reflection is the first peak from a two-dimensional hexagonal lattice (d_{10}), the cell dimension $a = 56.8$ Å (according to $a = 2d_{10}/\sqrt{3}$, where $d_{10} = 49.2$ Å). In the case where this reflection arises from cylindrically averaged interference between only a pair of objects separated by distance *a*, the intensity maximum occurs at the primary peak of J_0, where $2\pi aR = 7.037$; therefore, $a = 55.1$ Å. Thus the separation of the objects is within the range 55–57 Å. This is slightly smaller than the 60–70-Å fiber size observed by electron microscopy of negatively and positively stained samples.

Compared to the prominent arc at 49 Å, the three reflections at 19.0-, 13.7-, and 8.9-Å spacings were diffuse and had more uniform, circular intensity distributions. The reciprocal separation between 13.7 Å and 8.9 Å was used to estimate that the separation between two cylindrically averaged pair of objects was ~28 Å. It appears, therefore, that

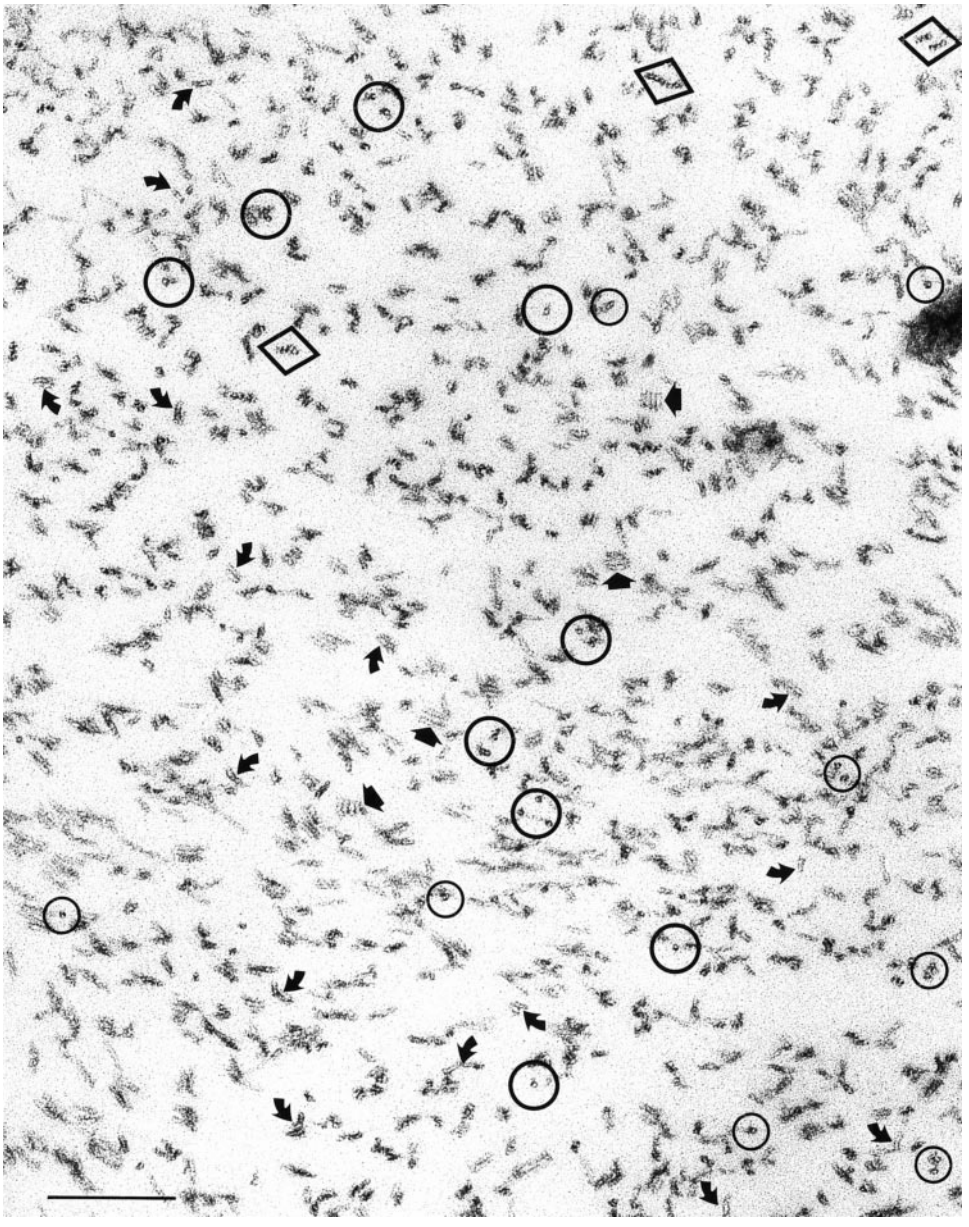

FIGURE 4 Electron micrograph of thin-sectioned preparation. A sample of Aβ(1–40) (synthesized by Dr. D. B. Teplow, Harvard Medical School), after 1 week of storage, displayed a tubular structure (~60 Å in diameter) with an electron-lucent center. Note the circular profiles where the fibers have been cut in cross section (*open circles*), the straw like outlines where the fibers were cut longitudinally (*curved arrows*), parallel alignment of closely apposed fibers (*straight arrows*), and cross-sectional views of such arrays (*open diamonds*). Scale bar, 1000 Å.

the three broad equatorial reflections at wide angle may arise from sampling of a very broad intensity maximum centered in this region.

Based on these considerations, we suggest the following model: pairs of β-sheets, with an intersheet distance of ~9 Å, build up a tubular cylinder (or protofilament; see below). The β-sheets are centered at radii $r_1 \approx 14$ Å (28 Å/2) and $r_2 \approx 5$ Å, respectively. This model is similar to the one proposed in our low-resolution studies of the shorter peptide Aβ(1–28) (Kirschner et al., 1987), and in recent x-ray analysis of transthyretin (TTR) amyloid (Blake and Serpell, 1996). When calculated with $r_1 = 14.3$ Å and $r_2 = 5.3$ Å, this model gives three broad equatorial reflections at spacings of 22, 13, and 8.9 Å, as shown in Fig. 6. The spacings of these reflections are determined mostly by the outer radius of the cylinder and are much less sensitive to the inner radius. The apparent intersheet reflection at 8.9 Å on the film does not correspond directly to the actual intersheet distance because of the cylindrical symmetry.

A single 28-Å-wide tubular cylinder, as described above, does not by itself account for the strong low-angle reflection at 49.2 Å. This intensity maximum derives, rather, from cylindrically averaged interference between objects that are separated by a distance of ~55 Å. Because negative staining shows that the fiber width is ~70 Å, the 28-Å-wide tubular structure would be a protofilament of the fiber. The arrangement of protofilaments along a circle with radius $r_o = 55$ Å/2 would account for both the small-angle and wide-angle reflections. From the geometrical constraint of $r_s = r_o \sin(\pi/N)$, where r_s(= 14.3 Å) and r_o(= 55 Å/2) are radii of the protofilament and fiber, respectively, the maximum number N of protofilaments is 5.7.

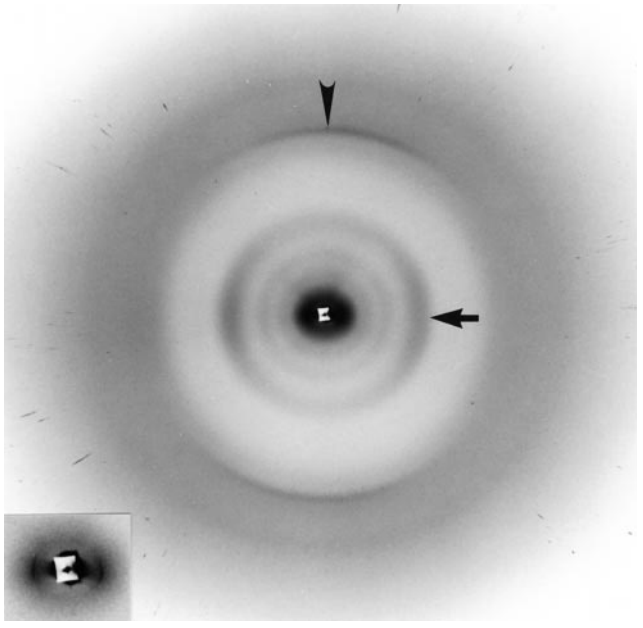

FIGURE 5 X-ray diffraction pattern from Aβ(1–40). The exposure time was 113 h, and the specimen-to-film distance was 71.8 mm. The spacings of the predominant reflections observed on the equator (E) and meridian (M) are 49.2 Å (E), 19.0 Å (E), 13.7 Å (E), 8.9 Å (E, *arrow*), 4.7 Å (M, *arrowhead*), and 3.8 Å (M). The inset shows, at higher magnification, the sharply arced reflection at 49.2 Å spacing.

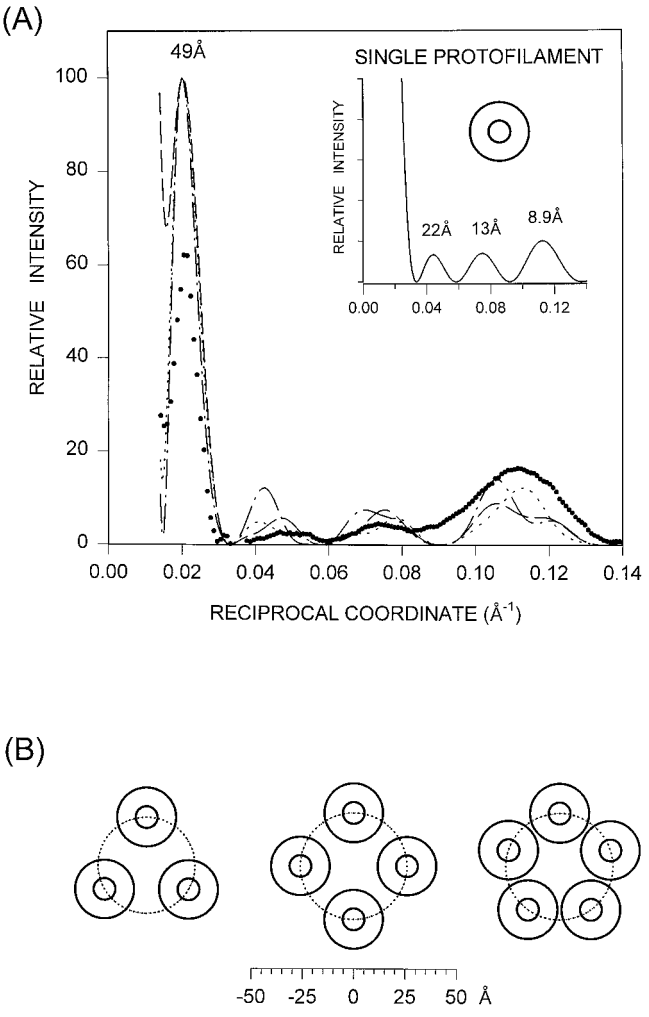

FIGURE 6 Modeling of the equatorial x-ray diffraction data from Aβ(1–40). (*A*) Experimental and calculated equatorial intensities for single (*A*, *inset*) and multiple (*B*) tubular protofilaments. For the latter, the protofilaments were arranged on the circumference of a circle whose radius was consistent with the first interference peak at 49.2 Å (see text for details). To reveal the low-angle region at ~0.02 Å^{-1}, densitometer traces of the first and second films were scaled and combined. The background was subtracted as described in Materials and Methods. Points (●), Experimental data; — —, three protofilaments; – – –, four protofilaments; — - —, five protofilaments.

The calculated intensity for a fibril consisting of 3, 4, and 5 protofilaments arranged on a circle of radius r_o is shown in Fig. 6. Radii of 23.5 Å for three protofilaments and 26 Å for four or five protofilaments were found by fitting the first interference peak to the observed position at 49.2 Å spacing. A fibril model consisting of only two protofilaments did not give any peak in this region, and a model consisting of six protofilaments was not plausible, because of steric considerations. These calculations show that the reflection at 49.2 Å may arise from protofilament interference, but the calculated intensity is stronger than the observed one. A disorder effect, not yet identified, may result in a smaller observed intensity of the 49.2 Å reflection, and may also reduce the influence of interference on the reflections at 22-, 13-, and 9-Å spacings. The intensity maxima at ~50 Å could also arise from interfibril interference as fibrils become closely packed in samples that are very concentrated.

Although the parameters are not optimized against the observed intensity, a likely model for the Aβ(1–40) assembly is that the 70-Å tubular fiber (average diameter) is made up of three, four, or five protofilaments and the individual protofilament is a ~30-Å-wide tubular structure whose wall is composed of a tilted array of β-chains. Although this symmetrical cross-sectional model is not ideally consistent with the twisted fiber, the cross section of which would be asymmetrical, the equatorial x-ray analysis provides an approximate model for both straight and twisted fibers.

DISCUSSION

Relating birefringence in drop test to magnetic orientation of fibrils

Anisotropically shaped macromolecular assemblies can be induced to orient by a strong magnetic field. The origin of the physical torque in proteins or polypeptide assemblies is diamagnetism of oriented aromatic groups (Pauling, 1936) and of oriented planar peptide bonds (Worcester, 1978; Pauling, 1979). In general, protein structures with substantial amounts of parallel α-helices will orient with the helices parallel to the magnetic field, whereas in β-pleated sheets the orientation of aromatic side chains plays a major role in the orientation of the structure as a whole.

The diamagnetic susceptibility that can be calculated from the x-ray diffraction patterns of different, oriented macromolecular assemblies is much larger than would be expected for a single assembly, suggesting that the group of assemblies orients cooperatively (Makowski, 1988). Thus, as pointed out in this paper, although an individual assembly may exhibit little or no orientation in a magnetic field, liquid crystalline domains consisting of several thousand particles are likely to orient.

These considerations can be used to explain the correlation between the drop test results and the magnetic orientation of the Aβ assemblies. During the drying of a drop of the peptide solution, the surface tension causes protein to concentrate in the circular perimeter of the drop (Fig. 1, *a* and *b*). Surface tension tends to align individual fibrils, whereas thermal effects tend to disorient them. In the case of cooperative domains consisting of parallel fibrils, the surface tension dominates the thermal effects, and so the domains show a net orientation along the periphery of the drop. Thus the birefringence in the drop test and the magnetic orientation of the preparations both likely depend on the formation of liquid crystalline domains. Long-term storage of the peptide solution in the cold ("aging") may promote formation of such domains by slowing the fibril growth and generating more uniform lengths of fibrils. In the case of Aβ(11–25), domains of parallel fibrils form within hours, whereas with Aβ(1–40), the process may require weeks or months.

Tilted β-chains

The β-structure in the current study of Aβ(1–40) showed a tilted array of orthogonal β-crystalline units in which the fiber grows in the (210) direction as opposed to the (200) (or strictly H-bonding) direction. Such tilted β-chains, having different extents of tilt angle, have been reported for different proteins. Previously, an immunoglobulin array in a single crystal showed formation of an infinite β-sheet arrangement where the β-chains were tilted from the direction normal to the long axis of the β-sheet (Schiffer et al., 1985). Studies of adenovirus fiber (Stouten et al., 1992) and transthyretin (TTR) (Hamilton et al., 1996) also show similar tilted chains. A recently reported twisted β-structure for TTR amyloid fibers (Blake and Serpell, 1996) describes a pair of polyalanine-like β-chains separated by ~10 Å in a helical array with a 115-Å pitch, with the β-chains running normal to the fiber direction.

Amphipathic nature of the sequence may produce twisted fiber

The sequence of peptide Aβ(1–40) is shown in Fig. 7. The pattern of different physical-chemical attributes (e.g., hydrophobicity, polarity, charge, side-chain size) in the Aβ(1–40) sequence was analyzed by methods involving Fourier transform and averaging (Inouye and Kirschner, 1991). The secondary structures (α-helix, α; β-structure, β; coil, c, and turn, t) were predicted according to Chou-Fasman (CH) (1978) and Garnier's (G) method with a zero decision constant (Garnier et al., 1978). The atomic coordinates (deposited in the Brookhaven Protein Data Bank, ID 1AML) were determined by solution NMR (Sticht et al., 1995). The authors (Sticht et al., 1995) (S) assigned two helices from the atomic coordinates in the sequences at Gln^{15}-Asp^{23} and Ile^{31}-Met^{35}. The first helix was predicted by the methods of Chou-Fasman and Garnier, whereas the second helix was not predicted by any method.

Asp-Ala-Glu-Phe-Arg-His-Asp-Ser-Gly-Tyr-Glu-Val-His-His-Gln-

	1	2	3	4	5	6	7	8	9	10	11	12	13	14	15
CF	α	α	α	α	-	t	t	-	β	β	α	β	α	α	β
G	α	α	α	α	α	c	c	t	t	t	t	c	c	α	α
S														α	α

Lys-Leu-Val-Phe-Phe-Ala-Glu-Asp-Val-Gly-Ser-Asn-Lys-Gly-Ala-

	16	17	18	19	20	21	22	23	24	25	26	27	28	29	30
CF	β	β	β	α	α	α	-	t	-	t	t	t	α	β	β
G	α	α	α	α	α	α	α	α	c	c	c	c	c	c	c
S	α	α	α	α	α	α	α	α							

Ile-Ile-Gly-Leu-Met-Val-Gly-Gly-Val-Val

	31	32	33	34	35	36	37	38	39	40
CF	β	β	β	β	β	β	β	-	-	-
G	β	β	β	β	β	β	β	β	β	β
S	α	α	α	α	α					

FIGURE 7 The sequence of peptide Aβ(1–40) (See text for details).

A number of fibrillar assemblies formed by Alzheimer's Aβ analogs have been analyzed by x-ray diffraction (see Inouye et al., 1993), including the N-terminal hydrophilic and C-terminal hydrophobic domains. In addition to the twisted fibers observed for Aβ(1–40) (reported here), similar morphology has previously been found for the shorter peptide analogs near the hydrophobic C-terminus, i.e., Aβ(34–42) (Halverson et al., 1990), Aβ(22–35) (Fraser et al., 1991a), and Aβ(25–35) (Fraser et al., 1993). Aβ(22–35) shows twisted fibers with 50–60 Å for the minimum width, 120 Å for the maximum width, and 1100 Å for the pitch, which is most similar to the one observed here for Aβ(1–40). Aβ(34–42) assembles into fibers having a much larger width (85–95 Å) in the narrowest region, and Aβ(25–35) assembles into a larger sheet (150–500 Å wide). The subunit of this sheet appears to be a 30-Å-wide protofilament (Fraser et al., 1993) similar to the one discovered here for Aβ(1–40). From the correlation between fiber morphology and the primary sequence, it is likely that the twisted fiber in Aβ(1–40) may be related to the amphipathic nature of the residues at positions 22–35.

Because the x-ray diffraction patterns from the Aβ(22–35) and Aβ(25–35) assemblies (Fraser et al., 1991a, 1993) show powderlike concentric rings and do not allow definition of the fiber direction in terms of an orthogonal unit cell

of the β-sheet, it is not clear whether the amphipathic property of these peptides can be related to the tilting of the β-chain as observed in Aβ(1–40). Transformation from a twisted fiber to a straight fiber has been reported for Aβ(34–42) when it is treated by a denaturing agent (Halverson et al., 1990) and for Aβ(1–40) at high pH (Fraser et al., 1992). These data suggest that residues that are exposed to the medium have a crucial influence on the twisted fiber assembly.

A tubular ultrastructure has previously been seen in electron micrographs of cross-sectioned fibrils and has been determined by analysis of x-ray diffraction patterns from assemblies formed by the shorter, N-terminal hydrophilic Aβ peptides—e.g., Aβ(6–25), Aβ(11–28), and Aβ(1–28) (Kirschner et al., 1987; Fraser et al., 1991a,b; Inouye et al., 1993). Our finding that a multimeric array of protofilaments also constitutes the tubular fibril assembled from the longer, more physiological Aβ(1–40) suggests that this is a common structural motif in amyloid fibril organization.

Fiber structure and neurotoxicity

Both Aβ(1–40) and Aβ(25–35), which contain the sequence of Aβ(22–35), are neurotoxic in fiber form (Yan et al., 1996; El-Khoury et al., 1996), suggesting that the twisted form of the fiber or ribbon structure may harbor a molecular structure with a high affinity for the putative receptor. As indicated in the secondary structure prediction and NMR result (see above), the hydrophilic part is largely turn or coil, and the hydrophobic part is predicted to be in an extended β-chain (or was determined to be α-helical in solution). It is thus likely that the hydrophilic turn at position 22–35 (Gly^{25}-Ser^{26}-Asn^{27}-Lys^{28}) might be exposed on the surface of the Aβ(1–40) fiber and that this is the part that binds to the receptor site.

Within the same batch of peptide and even on the same EM grid two different fibers were observed, one twisted and the other straight. This is similar to the case for another hallmark structure in Alzheimer's disease, i.e., paired helical filament (PHF) (Crowther, 1991). The three-dimensional reconstruction of a PHF fiber from electron micrographs indicates that the two different forms arise from different assemblies of the subunits (Crowther, 1991). This may also be the case for the ~70-Å-wide, tubular Aβ(1–40) fiber, which is likely composed of 30-Å protofilaments, as indicated here. The diffraction from A(β1–40) shows an atypical tilt of the β-chains, which may underlie the macroscopic twist of the fibers (Chothia and Murzin, 1993). Because the fiber form of Aβ(1–40) as opposed to the soluble form is neurotoxic, the structure of the Aβ(1–40) fiber is significant neuropathologically. How different fiber assemblies can affect neurotoxicity via receptor affinity is an important question. Refined x-ray diffraction and electron microscopic image analyses with parallel studies of Aβ cytotoxicity will address this question.

We thank Dr. John E. Maggio for his generosity in providing us with the highly purified Aβ(1–40) peptide from QCB, and Dr. Walter Phillips for giving us access to the x-ray equipment in his laboratory at the Rosenstiel Center, Brandeis University (Waltham, MA).

The research was supported by an Alzheimer's Association Zenith Award to DAK, and by a research grant from the National Aeronautics and Space Administration (NAG8-1145).

REFERENCES

Barrow, C. J., A. Yasuda, P. T. Kenny, and M. G. Zagorski. 1992. Solution conformations and aggregational properties of synthetic amyloid beta-peptides of Alzheimer's disease. Analysis of circular dichroism spectra. *J. Mol. Biol.* 225:1075–1093.

Barrow, C. J., and M. G. Zagorski. 1991. Solution structures of beta peptide and its constituent fragments: relation to amyloid deposition. *Science.* 253:179–182.

Bernal, J. D., and I. Fankuchen. 1941. X-ray and crystallographic studies of plant virus preparations. *J. Gen. Physiol.* 25:111–165.

Blake, C., and L. Serpell. 1996. Synchrotron x-ray studies suggest that the core of the transthyretin amyloid fibril is a continuous β-sheet helix. *Structure.* 4:989–998.

Chothia, C., and A. G. Murzin. 1993. New folds for all-beta proteins. *Structure.* 1:217–222.

Chou, P. Y., and G. D. Fasman. 1978. Empirical predictions of protein conformation. *Annu. Rev. Biochem.* 47:251–276.

Crowther, R. A. 1991. Straight and paired helical filaments in Alzheimer disease have a common structural unit. *Proc. Natl. Acad. Sci. USA.* 88:2288–2292.

El-Khoury, J., S. E. Hickman, C. A. Thomas, L. Cao, S. C. Silverstein, and J. D. Loike. 1996. Scavenger receptor-mediated adhesion of microglia to β-amyloid fibrils. *Nature.* 382:716–719.

Fraser, P. E., L. K. Duffy, M. B. O'Malley, J. Nguyen, H. Inouye, and D. A. Kirschner. 1991a. Morphology and antibody recognition of synthetic β-amyloid peptides. *J. Neurosci. Res.* 28:474–485.

Fraser, P. E., D. R. McLachlan, J. T. Nguyen, C. A. Mizzen, and D. A. Kirschner. 1993. Structural modeling of Alzheimer Aβ peptide 25–35: comparison to α1-antitrypsin and implications for amyloid toxicity. *Neurodegeneration.* 2:155–163.

Fraser, P. E., J. T. Nguyen, H. Inouye, W. K. Surewicz, D. J. Selkoe, M. B. Podlisny, and D. A. Kirschner. 1992. Fibril formation by primate, rodent, and Dutch-Hemorrhagic analogues of Alzheimer amyloid β-protein. *Biochemistry.* 31:10716–10723.

Fraser, P. E., J. Nguyen, W. Surewicz, and D. A. Kirschner. 1991b. pH-dependent structural transitions of Alzheimer amyloid peptides. *Biophys. J.* 60:1190–1201.

Garnier, J., D. J. Osguthorpe, and B. Robson. 1978. Analysis of the accuracy and implications of simple methods for predicting the secondary structure of globular proteins. *J. Mol. Biol.* 120:97–120.

Geddes, A. J., K. D. Parker, E. D. T. Atkins, and E. Beighton. 1968. "Cross-beta" conformation in proteins. *J. Mol. Biol.* 32:343–358.

Halverson, K., P. E. Fraser, D. A. Kirschner, and P. T. Lansbury. 1990. Molecular determinants of amyloid deposition in Alzheimer's disease: conformational studies of synthetic β-protein fragments. *Biochemistry.* 29:2639–2644.

Hamilton, J. A., L. K. Steinrauf, B. C. Braden, J. R. Murrell, and M. D. Benson. 1996. Structural changes in transthyretin produced by the Ile 84 Ser mutation which result in decreased affinity for retinol-binding protein. Amyloid. *Int. J. Exp. Clin. Invest.* 3:1–12.

Inouye, H. 1994. X-ray scattering from a discrete helix with cumulative angular and translational disorders. *Acta Crystallogr.* A50:644–646.

Inouye, H., P. E. Fraser, and D. A. Kirschner. 1993. Structure of β-crystallite assemblies formed by Alzheimer β-amyloid protein analogues: analysis by x-ray diffraction. *Biophys. J.* 64:502–519.

Inouye, H., and D. A. Kirschner. 1991. Folding and function of the myelin proteins. *J. Neurosci. Res.* 28:1–17.

Kirschner, D. A., H. Inouye, L. K. Duffy, A. Sinclair, M. Lind, and D. J. Selkoe. 1987. Synthetic peptide homologous to β protein from Alzheimer disease forms amyloid-like fibrils in vitro. *Proc. Natl. Acad. Sci. USA.* 84:6953–6957.

Makowski, L. 1988. Preparation of magnetically oriented speciments for diffraction experiments. *In* Brookhaven Symposium—Synchrotron Radiation in Biology. R. M. Sweet and A. D. Woodhead, editors. New York, Plenum Press. 341–347.

Mattson, M. P., and R. Rydel. 1996. Amyloid ox-tox transducers. *Nature.* 382:674–675.

Nguyen, J. T., H. Inouye, M. A. Baldwin, R. J. Fletterick, F. E. Cohen, S. B. Prusiner, and D. A. Kirschner. 1995. X-ray diffraction of scrapie prion rods and PrP peptides. *J. Mol. Biol.* 252:412–422.

Oldenbourg, R., and W. C. Phillips. 1986. Small permanent magnet for fields up to 2.6T. *Rev. Sci. Instrum.* 57:2362–2365.

Pauling, L. 1936. The diamagnetic anisotropy of aromatic molecules. *J. Chem. Phys.* 4:673–677.

Pauling, L. 1979. Diamagnetic anisotropy of the peptide group. *Proc. Natl. Acad. Sci. USA*. 76:2293–2296.

Pike, C. J., A. J. Walencewicz, C. G. Glabe, and C. W. Cotman. 1991a. In vitro aging of beta-amyloid protein causes peptide aggregation and neurotoxicity. *Brain Res.* 563:311–314.

Pike, C. J., A. J. Walencewicz, C. G. Glabe, and C. W. Cotman. 1991b. Aggregation-related toxicity of synthetic beta-amyloid protein in hippocampal cultures. *Eur. J. Pharmacol.* 207:367–368.

Schiffer, M., C.-H. Chang, and F. J. Stevens. 1985. Formation of an infinite β-sheet arrangement dominates the crystallization behavior of lambda-type antibody light chains. *J. Mol. Biol.* 186:475–478.

Sticht, H., P. Bayer, D. Willbold, S. Dames, C. Hilbich, K. Beyreuther, R. W. Frank, and P. Esch. 1995. Structure of amyloid Aβ-(1–40)-peptide of Alzheimer's disease. *Eur. J. Biochem.* 233:293–298.

Stouten, P. F., C. Sander, R. W. H. Ruigrok, and S. Cusack. 1992. New triple-helical model for the shaft of the adenovirus fibre. *J. Mol. Biol.* 226:1073–1084.

Tibbitts, T. T., and D. L. D. Caspar. 1993. Deconvolution of disoriented fiber diffraction data using iterative convolution and local regression. *Acta Crystallogr.* A49:532–545.

Vainshtein, B. K. 1966. Diffraction of X-Rays by Chain Molecules. Elsevier Publishing Company, Amsterdam.

Worcester, D. 1978. Structural origins of diamagnetic anisotropy in proteins. *Proc. Natl. Acad. Sci. USA.* 75:5475–5477.

Yan, S. D., X. Chen, J. Fu, M. Chen, H. Zhu, A. Roher, T. Slattery, L. Zhao, M. Nagashima, J. Morser, A. Migheli, P. Nawroth, D. Stern, and A. M. Schmidt. 1996. Receptors for Alzheimer's RAGE and amyloid-β peptide neurotoxicity in Alzheimer's disease. *Nature.* 382:685–691.